High-Frequency Vibrations of the Simplest Benzylic Amide [2]Catenane

Marianna Fanti,[†] Charles-André Fustin,[‡] David A. Leigh,*[,§] Aden Murphy,[§] Petra Rudolf,*[,‡] Roland Caudano,[‡] Roberto Zamboni,[||] and Francesco Zerbetto*[,†]

Dipartimento di Chimica "G. Ciamician", Università degli Studi di Bologna, V. F. Selmi 2, 40126 Bologna, Italy, Laboratoire Interdisciplinaire de Spectroscopie Electronique, Facultes Universitaires Notre-Dame de la Paix, Rue de Bruxelles, B-5000 Namur, Belgium, Department of Chemistry, University of Manchester Institute of Science and Technology, Sackville Street, Manchester M60 1QD, U.K., Istituto di Spettroscopia Molecolare, Consiglio Nazionale delle Ricerche, Via Gobetti 101, Bologna, Italy

Received: October 8, 1997; In Final Form: May 5, 1998

Infrared and Raman spectroscopies along with molecular orbital calculations are used to study—for the first time—the vibrational motions of a topologically complicated chemical system, namely a [2]catenane of the benzylic amide type. Because of the intrinsic line width of the spectra, comparison of experiments and theory is only partially successful. The insight given by the simulations—which show that the C═O normal modes are delocalized while the N−H modes are localized—is, however, useful and makes us propose a simple model that explains both the larger line width of the spectra of the catenane with respect to those of the parent macrocycle and the great sensitivity of the infrared spectrum of the catenane to the environment. Examples of such sensitivity are the frequency shifts observed upon going from KBr to CsI, features not present in the case of the macrocycle.

Introduction

Through the pioneering work of Sauvage, Stoddart, and others,[1] catenanes (mechanically interlocked macrocycles) are becoming seen as important potential component structures for nanotechnology. One reason for this is that for catenanes composed largely of rigid aromatic units, the combination of the restriction in the freedom of motion of components in some directions (imposed by interlocking), together with that allowed in others, is similar to the degrees of freedom allocated to moving parts in machinery in the macroscopic world. Furthermore, their mechanically interlocked architectures allow catenanes to change the relative separation (and therefore the nature and degree of interaction) between pendant functionality on each macrocycle, by this potentially allowing switching "on" and "off" of particular properties in a manner not open to the majority of topologically trivial molecules. To develop applications of these molecules, it is clearly necessary to fully understand the nature of their inter- and intra-ring interactions. Apart from their structures, their characterization in terms of fundamental and induceable properties must *perforce* start with the study of the electronic and nuclear motions that reflect the different time-scale dynamics present in the system. Here we report the first study of the high-frequency vibrational states of a mechanically interlocked molecule, the benzylic amide [2]-catenane **1** (Figure 1). To the best of our knowledge, this is the first vibrational study of any catenane.

Large (i.e., ≥100 atoms) organic systems that contain conjugated repeat units can be loosely divided in two sets. The first consists of entirely conjugated molecules—polyenes, polythiophenes, and porphyrins, for example. In the second, one finds molecules whose conjugated moieties are separated by saturated bridges. In terms of properties, the difference between the two sets can be highly significant. Fully conjugated molecules cannot realistically be studied as the sum of their interacting fragments. Polyenes epitomize this kind of behavior.[2] In contrast, when the building blocks are divided by one or more sp^3 carbon atoms, as is the case with benzylic amide catenanes, perturbation theory can still hold and the molecular properties may be determined by analytical models in both the simplest cases of a "dimer" and even in the most complex case of an infinite chain. Difficulties—and implicitly a degree of interest—arise when the number and the roles of the interacting fragments vary.

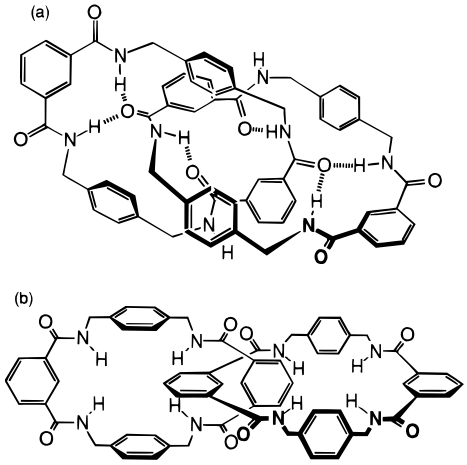

Figure 1. Benzylic amide [2]catenane **1**: (a) solid-state structure determined by X-ray crystallography and (b) ideal structure.

The prototypical benzylic amide [2]catenane **1** is the simplest member of a large family of molecules prepared through a self-assembly process serendipitously discovered at UMIST.[3] The system consists of four isophthalic diamide and four *p*-xylyl groups in the form of two identical macrocycles that are

[†] Università degli Studi di Bologna.
[‡] Facultes Universitaires Notre-Dame de La Paix.
[§] University of Manchester Institute of Science and Technology.
[||] Consiglio Nazionale delle Ricerche.

S1089-5639(97)03275-1 CCC: $15.00
Published on Web 06/29/1998

mechanically interlocked and can be viewed as the sum of two sets of four isolated conjugated units. To add further similarity, every moiety is basically a derivatized phenyl group. Owing to the interlocked structure, the interactions between various individual units cannot be assumed to be the same. For example, the interaction of a fragment with a similar fragment in the same macrocycle differs from the interaction between fragments that are not located in the same macrocycles; the first is determined by a combination of through-space and through-bond interactions while the second is only through-space, although it can have an additional contribution brought about by hydrogen bonding. Furthermore, the environments and conformations of each group are not the same, at least in the solid state.[3] Mechanical and electronic interactions can occur and modify the properties of the catenane with respect to those of the macrocyclic monomers. Vibrational spectroscopy is particularly well-suited to provide information regarding mechanical interactions. The vibrational frequencies, and their intensities or cross sections, are a function of the normal modes which, in turn, image the nuclei dynamics. Two main scenarios—and their combinations—can conceivably emerge from the spectra and their analysis: in the first, interaction between the fragments spreads the vibrational frequencies of a group over a certain range, and in the second, the different environments experienced by each spectroscopically active group sets them apart from one another. In the first instance, spectroscopy becomes a probe of the interaction *between* the moieties, in the second, it becomes a probe of the *local environment* of the groups.

The work carried out in this paper presents the results of a combination of experimental and computational, or modeling, techniques aimed at obtaining a picture of the interactions and the high-frequency vibrational dynamics of the simplest octabenzamide [2]catenane, **1**. The infrared and Raman spectra are recorded at standard resolution and compared with the result of molecular orbital calculations. The emerging picture of a strong and easily modified interplay between local vibrational oscillators is supported by the a simple model and the significant differences that appear in the infrared spectra of the catenane in two different matrixes.

Experimental Procedure

Preparation. [2] (1,7,14,20-Tetraaza-2,6,15,19-tetraoxo-3,5,9,12,16,18,22,25-tetrabenzocyclohexacosane)-(1′,7′,14′,20′-tetraaza-2′,6′,15′,19′-tetraoxo-3′,5′,9′,12′,16′,18′,22′,25′-tetrabenzocyclohexacosane) Catenane (1). To a stirred solution of triethylamine (1.19 g, 18.9 mmol) in anhydrous (stabilized with amylenes, not ethanol) chloroform (130 mL) under argon were added isophthaloyl dichloride (0.87 g, 4.3 mmol) in anhydrous chloroform (130 mL) and *p*-xylylene diamine (0.58 g, 4.3 mmol) in anhydrous chloroform (130 mL) simultaneously, over 30 min using motor-driven syringe pumps. The mixture was allowed to stir overnight and then filtered. The filtrate was washed with 1 M aqueous hydrochloric acid (3 × 200 mL), then 5% aqueous sodium hydroxide (3 × 200 mL), and finally water (3 × 200 mL). The organic layer was then dried over anhydrous magnesium sulfate and concentrated under reduced pressure to afford 0.23 g (20.1%) of catenane (**1**); mp 315 °C (decomposes); ^{1}H NMR (300 MHz, [D$_6$]DMSO) δ 8.62 (8H, s), 8.05 (4H, d), 7.88 (8H, dd), 7.50 (4H, t), 6.75 (16H, bs), 4.01 (16H, bs); ^{13}C NMR (75 MHz, DMSO-d_6) δ 168.9, 141.3, 138.4, 133.7,132.4, 130.8, 130.0, 46.9; FAB-MS (*m*NBA matrix): *m*/*z* 1065 $(M + H)^+$, 533 $(M/2 + H)^+$.

Infrared Spectroscopy. The standard resolution infrared spectra were recorded with a Fourier Transform spectrometer Brüker 113V working under vacuum (10^{-1} Torr). The interferometer was of the Genzel type, and the resolution was set to 1 cm^{-1}. A standard DTGS detector equipped with KBr and polyethilene windows was used. The catenane or the parent macrocycle powder was mixed with 200 mg of CsI or KBr and pressed into a pellet. The infrared spectra for the comparison between the KBr and the CsI matrixes were collected with a Fourier transform spectrometer BIO-RAD FT 60A equipped with a KBr beam splitter and a DTGS detector. The inferometer was of Michelson type, and the resolution was set to 2 cm^{-1}. The samples were again pellets of CsI or KBr with a 1.25% concentration in weight of the catenane or the parent macrocycle.

Raman Spectroscopy. The Raman spectrometer used in this study was a Brüker RFS 100 equipped with a Nd:YAG laser working at 1064 nm operated at a power of 260 mW. The resolution was set to 2 cm^{-1}. A Ge diode operating at liquid nitrogen temperature was used as a detector. The Raman measurements were performed in the backscattering configuration. The catenane powder was pressed into a small hole in a metallic pellet.

Theoretical Background

The semiempirical calculations carried out for this work were performed with the Gaussian92 suite of programs.[4] This package includes both semiempirical and ab initio procedures. In the semiempirical part, the Hessian matrix—i.e., the matrix of the second derivatives of the energy with respect to nuclear displacements—is obtained by numerical differentiation of the energy gradients. Calculation of this matrix is the rate-determining step for vibrational frequencies and normal modes. Subsequent projection of the normal modes onto the vector of the dipole moment derivatives gives the infrared intensities. This part of the program does not calculate the Raman cross sections. They can be calculated ab initio at the Hartree−Fock level, but not at the semiempirical level. The numerical differentiation used to calculate the Hessian matrix, however, can be utilized advantageously to minimize the effort required when one extends the computer code to the Raman activities. The vector of the Cartesian derivatives with respect to the nuclear displacements can be readily obtained if at each step one adds the evaluation of the polarizability. Subsequent projection of the normal modes onto this vector furnishes the Raman activities. More in detail, the Raman cross section is proportional to $\partial \alpha_i^n/\partial Q$, where α is the polarizability tensor and $\{Q\}$ is the set of the vibrational normal modes. The procedure to calculate α[5] is general and can be applied both to semiempirical and ab initio wave functions. One can start from the classic expression for the energy perturbation due to an external monochromatic field, $F = F_0(e^{i\omega t} + e^{-i\omega t} + 1)$

$$E(F) = E - \mu_a F^a - \frac{1}{2!}\alpha_{ab}F^aF^b - \frac{1}{3!}\beta_{abc}F^aF^bF^c - \ldots \quad (1)$$

where the sum over repeated indices is implied. In eq 1, μ_a, α_{ab}, and β_{abc} stand for dipole moment, polarizability, and hyperpolarizability. The term $H^a = \mu_a F^a$ is the perturbation responsible for the polarizability, in which

$$\mu = -\sum er_j \quad (2)$$

where the sum runs over all the electrons. Quantum chemically, the energy variation caused by the electric field can be written as

$$\alpha_{ab} = -Tr(H^a(D^b(F))) \tag{3}$$

where H^a is the dipole moment matrix in the atomic orbital basis $\{\chi\}$ whose matrix elements read

$$H^a_{st} = -\langle\chi_s|es|\chi_t\rangle \tag{4}$$

and $D^b(F)$ is the density matrix perturbed along the b direction

$$D^b(F) = C^b(F)\, nC^*(0) + C(0)\, nC^{b*}(F) \tag{5}$$

where C is the matrix of the molecular orbitals, $C(0)$ and $C(F)$ are the orbitals before and after the field is switched on, and n is the occupation matrix. The perturbed molecular orbitals are calculated as

$$C^b(F) = C^0(0)U^b(F) \tag{6}$$

where the matrix elements of U are expressed in terms of the auxiliary matrix G as

$$U^b_{ij}(F) = \frac{G^b_{ij}(F)}{\epsilon^0_j - \epsilon^0_i} \tag{7}$$

where i and j refer to occupied and unoccupied orbitals and ϵ^0_i is the unperturbed energy of the orbital. The auxiliary matrix G represents the perturbation in the molecular orbital basis. This scheme can converge to the final result of eq 3 via an iterative procedure:

first, the dipole moment matrix in the atomic orbital basis is built;

second, the matrix is rotated in the molecular orbital basis to give G, and subsequently U, C, and D;

third, the new perturbation is calculated with the orbitals obtained by diagonalization of the perturbed Hartree−Fock matrix, $F^b(F) = H^b + D^b(F)[2J^0 - K^0]$, where J and K are the Coulomb and exchange matrixes;

fourth, the convergence is checked, and if not achieved steps 2 and 3 are repeated.

A detailed analysis of frequency-dependent and static properties calculated with this model up to third order has been given before.[5] After numerical differentiation of the polarizability with respect to the Cartesian coordinates, the vector is projected along the normal modes. The Raman intensities, $I_T(\text{obs}\perp)$, for the total light scattered in a direction perpendicular to that of the electric vector of the incident beam are obtained as

$$I_T(\text{obs}\perp) = \text{const}(45\bar{\alpha}^2 + 7\beta_s^2) \tag{8}$$

where the constant is proportional to the fourth power of the field and

$$\bar{\alpha} = {}^1/_3(\alpha_{11} + \alpha_{22} + \alpha_{33}) \tag{9}$$

and

$$2\beta_s^2 = \frac{1}{2}\sum_{ij}|\alpha_{ii} - \alpha_{jj}|^2 + \frac{3}{4}\sum_{ij}^{i\neq j}|\alpha_{ij} + \alpha_{ji}|^2 \tag{10}$$

The theory of the Raman scattering in terms of the polarizability tensor can be found in Califano.[6] Calculations of the Raman cross sections along the scheme given above have been successful in the simulation of the spectra of C_{60}, C_{70},[7] and two isomers of C_{78}.[8]

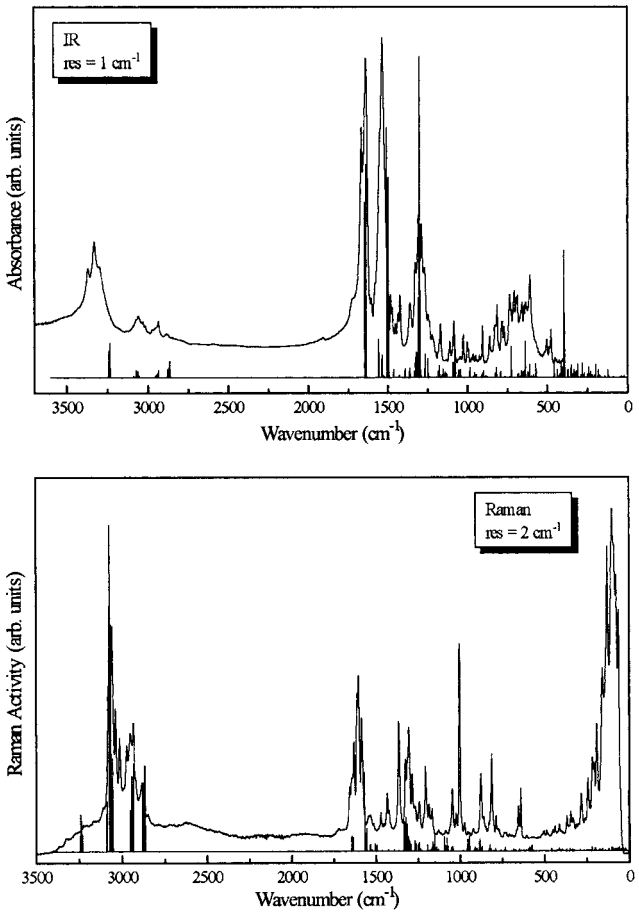

Figure 2. Top: Standard resolution infrared spectrum of benzylic amide [2]catenane **1**. The stick spectrum represents the MNDO frequencies scaled according to eq 11 and the corresponding intensities. Bottom: Raman spectrum of benzylic amide [2]catenane **1**. The stick spectrum represents the MNDO frequencies scaled according to eq 11 and the corresponding cross sections.

It is important to emphasize that the approach outlined above cannot be used in the pre-resonant and resonant regimes where the largest contribution comes from the Franck−Condon factors of the resonant state. The Raman experiments reported in this work are strictly in the off-resonant regime, and as such the procedure outlined above is deemed adequate.

Results and Discussion

In this work, we present the first characterization of the high-frequency vibrational motions of the parent benzylic amide [2]-catenane. The intent is to obtain information on the interaction that exists in the molecule and that can be probed by infrared and Raman spectroscopy. To this end, we proceed in three steps: first, we present the spectra in rather general terms and compare them with molecular orbital calculations of the frequencies and intensities. Then we set up a very simple model that naturally yields a possible origin of line-broadening—one of the causes of the difficulties in the comparison of theory and experiments. Finally, the consequences of the model are discussed in terms of the different behavior shown by the catenane and its parent macrocycle in different salt matrixes.

Introducing the Spectra. Cursory inspection of the spectra in the high-frequency region gives a fair amount of general information. The most intense, identifiable bands of the infrared spectrum shown at the top of Figure 2 can be assigned[9] as follows:

(i) 3368, 3330, 3300 cm^{-1} N−H stretchings,

(ii) 3058 cm^{-1} (group of peaks) aromatic C−H stretchings,

(iii) 2934 cm^{-1} (group of peaks), 2886 cm^{-1} aliphatic C−H stretchings,

(iv) 1665, 1637 cm^{-1} C═O stretchings,

(v) 1533 cm^{-1}, amide II band, C−N stretchings plus N−H bendings,

(vi) 1302 cm^{-1}, amide III band, C−N stretchings plus N−H bendings, and

(vii) the remaining bands at 1482, 1472, 1452, 1433, 1424, 1360, 1326, 1287, 1268, 1247, 1220, 1168, 1109, 1084, 1025,-1000, 993, 904, 859, 813, 786, 779, 769, 734,705, 692, 686, 657, 641, 634, 605, 502, and 477 cm^{-1} are variously due to C−C stretchings, CCH and CCC bendings, further amide bands, and out-of-plane distortions.

The most intense bands of the Raman spectrum shown at the bottom of Figure 2 can be assigned as:

(i) 3072, 3057, 3037 cm^{-1} aromatic C−H stretchings,

(ii) 2912, 2996 cm^{-1} aliphatic C−H stretchings,

(iii) 1657, 1632 cm^{-1} C═O stretchings,

(iv) 1613, 1603, 1586 cm^{-1} phenyl deformation, and

(v) 1471, 1432, 1420 cm^{-1} C−H_2 deformation, and

(vi) the remaining bands at 1363, 1325, 1305, 1285, 1268,-1242, 1206, 1185, 1166, 1046, 1002, 972, 954, 877, 811, 787, 698, 669, and 641 cm^{-1} are variously due to C−C stretchings, CCH and CCC bendings, further amide bands, and out-of-plane distortions.

The inspection given above of the spectra furnishes general information on the molecular structure. Insight into the properties and the dynamics of the molecule requires either the decomposition of the bands in the constituent transitions or an appropriate simulation based on quantum chemical methods.

The Calculations. The vibrational frequencies and normal modes calculations along with the simulation of the infrared intensities and Raman cross sections were performed at the MNDO level (see Table 1).[10] Straightforward plotting of the spectra off the computer output would be highly desirable, but for a molecule of this size, it is not a realistic possibility with the presently available quantum chemical models. Standard procedures usually employed for far smaller molecules entails the scaling of the force constants through fitting of the experimental frequencies. The large line width of the spectra made unlikely the identification of a number of frequencies sufficient to guide a fitting. We therefore decided, as a first step to improve agreement between experiment and theory, to scale the vibrational frequencies. Quite often, a common scaling factor of 0.9 has been used.[8] We soon found that this was hardly useful for benzylic amide [2]catenane. Resorting to a more elaborate scaling function gave the best agreement when the frequencies were obtained as

$$\nu_{new} = 0.9\nu_{calc} - A\nu_{calc}e^{(\nu_{calc}-\nu_0)^2/\alpha^2} \qquad (11)$$

where ν is the vibrational wavenumber in cm^{-1}, A is 0.116, ν_0 is 2100 cm^{-1}, and α is 150 cm^2. The behavior of this function is such that the largest effects are observed for the C═O stretching region; they then taper off toward zero or toward frequencies too high to be fundamentals. A similar approach, although with a different function, was used elsewhere[11] to improve the agreement between inelastic neutron scattering experiments and their semiemprical simulation. With the frequencies obtained by this scaling equation together with the calculated infrared intensities and Raman cross sections, one can plot the stick spectra shown in Figure 2 together with their experimental counterparts. The agreement can be considered satisfactory. One should be aware of the fact that eq 11 is totally empirical and is used to improve the match between calculations and experiments. The rationale behind this approach is the observation that the inaccuracy of theory is largest in the C═O stretching region and that there is a smooth convergence toward the experimental values at low and high wavenumbers. While, this scaling function may not be general it is expected, however, that it can be transferable to other derivatives of the benzylic amide. The two most notable failures of the quantum chemical simulation are (1) the small infrared intensity in the X−H region (which is likely to require the description of the anharmonicity in the dipole moment surface[12]) and (2) the lack of the prominent Raman line located around 1000 cm^{-1}. It should be noticed, however, that this line is likely to be the breathing mode of the phenyl rings and as such it owes its intensity to Franck−Condon contributions that are not present in the TDHF model employed by us. On the bright side, we notice that the simulations account well for the three main bands of the infrared region between 1000 and 1700 cm^{-1} and can describe the Raman X−H region and the second most intense Raman region around 1600 cm^{-1}. Apart from the comparison between experiment and simulations, the calculations provide the forms of the normal modes. Their analysis showed that they are, in general, quite delocalized over the entire molecule. An exception was found for the N−H stretches, which are strongly localized.

The Broadening of the Bands. To obtain a better insight in the spectra, one should consider the sources of line broadening. In a system as large as the present one—made up by 136 atoms—the information conveyed by the spectroscopic measurements is blurred by the sheer size of it. In principle, because of the low symmetry of the molecular point group, all of the 402 fundamentals can contribute to the response. The low symmetry is intrinsic to the system that is stabilized by the hydrogen bonds and the π-electron stacking interactions that have their most evident manifestation in the presence of only one carbonyl group pointing toward the center of each macrocycle.[3] Intrinsically, the different environments experienced by each local oscillator can make their frequencies vary from the pristine value. For instance, the stretching frequencies of the eight COs will depend on whether they form a single hydrogen bond, a bifurcated hydrogen bond, or no hydrogen bond. Importantly, the interaction with the environment make the groups different and can localize the vibrational modes.

Even before the interaction with the environment, a simple mechanism can be shown to affect the frequencies of the different types of active groups. To introduce it, one can start by looking at the two components of the system, i.e., the individual macrocycles, and study one of them in a high-symmetry regime. For sake of simplicity, we consider the four C═O stretches—a similar argument with different parameters would hold for the other vibrational chromophores—and assume that to zeroth order they are equivalent (high-symmetry hypothesis). Because of the presence of the *p*-xylyl and isophthaloyl groups, two interactions are present between the groups; we call them α and β. To maintain the model qualitative, we do not assign them. In the macrocycle, every C═O stretch has one α and one β interaction. One can write the Hamiltonian matrix associated to this problem, which reads

$$H = \begin{pmatrix} D & \alpha & 0 & \beta \\ \alpha & D & \beta & 0 \\ 0 & \beta & D & \alpha \\ \beta & 0 & \alpha & D \end{pmatrix} \qquad (12)$$

where H is the mass-weighed force constant matrix, D is the

TABLE 1: Summary of the MNDO Calculations: Unscaled Vibrational Wavenumbers, $\tilde{\nu}$, Infrared Intensities, ir, and Raman Cross Sections, R

$\tilde{\nu}$	9	12	15	19	21	23	25	28	29	31	31	34
ir	0	0	0	0	1	5	0	2	1	0	0	2
R	0	0	1	1	1	0	7	4	6	2	2	3
$\tilde{\nu}$	36	38	40	41	42	47	48	53	54	65	66	70
ir	2	0	0	0	5	0	3	1	0	1	0	1
R	1	6	1	4	1	3	1	2	7	0	14	11
$\tilde{\nu}$	72	77	79	87	88	91	95	96	99	103	107	111
ir	0	0	0	0	0	1	2	2	2	0	1	0
R	3	4	8	7	2	8	1	1	6	5	1	11
$\tilde{\nu}$	115	117	133	137	155	159	176	178	189	191	195	196
ir	0	1	8	26	5	5	1	1	5	0	1	8
R	3	12	3	8	1	2	0	9	0	5	5	3
$\tilde{\nu}$	203	203	221	221	227	228	243	245	255	256	267	269
ir	16	10	27	19	2	5	2	8	20	14	12	35
R	2	1	9	0	3	7	8	15	2	2	3	2
$\tilde{\nu}$	274	278	281	281	299	299	311	313	322	323	344	344
ir	10	12	5	1	6	10	22	50	9	1	20	47
R	2	2	2	3	2	1	0	2	0	4	0	1
$\tilde{\nu}$	354	354	363	364	368	368	369	369	372	372	374	374
ir	20	2	17	10	19	17	0	1	26	0	7	7
R	1	1	4	4	0	1	0	0	2	1	4	1
$\tilde{\nu}$	380	382	389	390	411	412	415	416	435	436	441	445
ir	11	0	44	0	3	26	21	2	222	5	438	4
R	0	3	2	6	4	2	0	0	1	3	4	1
$\tilde{\nu}$	449	456	459	460	470	477	482	486	486	489	507	508
ir	35	4	48	24	13	3	2	7	22	1	51	0
R	1	4	5	8	5	3	0	2	0	1	1	6
$\tilde{\nu}$	509	511	632	634	636	636	641	641	641	642	651	652
ir	10	1	27	3	9	49	0	0	0	1	9	7
R	4	8	2	1	1	2	17	3	6	6	5	3
$\tilde{\nu}$	655	656	662	663	677	677	677	678	691	691	708	709
ir	1	1	1	4	5	31	14	1	12	8	125	40
R	12	1	2	4	1	2	0	2	1	4	1	2
$\tilde{\nu}$	710	711	715	715	723	723	735	736	746	746	757	758
ir	29	6	3	9	11	11	23	17	1	1	13	1
R	0	1	1	1	1	5	1	1	1	1	0	5
$\tilde{\nu}$	762	762	808	808	814	815	844	844	850	850	880	880
ir	5	5	108	51	0	2	1	1	0	4	7	9
R	1	2	0	1	13	1	2	2	1	1	4	3
$\tilde{\nu}$	880	881	908	908	914	916	916	916	917	918	968	969
ir	6	3	31	5	1	4	0	3	15	0	0	1
R	2	2	1	6	1	2	10	10	4	11	17	1
$\tilde{\nu}$	977	977	981	981	986	987	1000	1001	1002	1003	1004	1004
ir	1	1	2	3	5	2	5	18	4	0	0	0
R	2	5	11	31	3	32	7	2	2	5	1	1
$\tilde{\nu}$	1006	1007	1013	1013	1018	1019	1041	1041	1041	1041	1049	1049
ir	14	5	3	4	0	3	0	0	0	0	10	2
R	6	2	3	11	3	4	1	0	0	0	6	3
$\tilde{\nu}$	1050	1050	1051	1051	1053	1053	1061	1061	1062	1062	1064	1065
ir	3	7	0	2	0	1	0	1	5	11	2	0
R	3	40	2	50	1	10	0	3	35	3	0	22
$\tilde{\nu}$	1066	1066	1093	1093	1094	1094	1160	1160	1162	1163	1171	1171
ir	2	4	9	6	5	28	18	11	1	1	6	4
R	1	8	1	3	1	1	2	4	8	9	3	9
$\tilde{\nu}$	1173	1173	1194	1194	1199	1199	1210	1211	1212	1212	1215	1215
ir	21	5	44	2	61	41	6	21	27	25	24	4
R	4	5	1	15	13	32	5	7	7	11	5	14
$\tilde{\nu}$	1215	1216	1256	1256	1260	1260	1267	1267	1272	1273	1279	1279
ir	5	9	6	6	15	2	16	4	12	12	8	0
R	19	13	3	3	1	2	2	12	8	9	5	18
$\tilde{\nu}$	1280	1280	1282	1282	1286	1286	1291	1291	1293	1293	1295	1296
ir	1	1	30	1	7	4	1	4	0	0	2	1
R	6	32	1	4	15	7	3	1	16	15	17	10
$\tilde{\nu}$	1306	1306	1314	1315	1328	1328	1368	1368	1368	1368	1374	1374
ir	21	21	4	19	1	1	0	0	1	1	1	2
R	1	6	1	1	10	12	2	2	1	1	8	2
$\tilde{\nu}$	1375	1375	1384	1384	1389	1389	1405	1405	1410	1410	1436	1437
ir	3	1	13	0	25	69	1	82	11	21	1	24
R	1	2	7	23	12	23	23	2	23	13	10	24
$\tilde{\nu}$	1442	1444	1446	1447	1450	1451	1453	1453	1457	1457	1461	1461
ir	300	829	257	865	48	1	252	24	62	37	4	8
R	15	4	20	16	15	27	16	34	3	11	10	33
$\tilde{\nu}$	1462	1462	1469	1469	1472	1472	1475	1475	1483	1483	1513	1513
ir	20	51	16	72	71	25	31	24	6	16	10	22
R	78	17	68	51	11	20	26	59	76	27	0	0
$\tilde{\nu}$	1515	1516	1546	1547	1547	1547	1586	1586	1587	1587	1626	1626
ir	3	29	7	25	2	1	3	5	2	2	27	1
R	1	2	2	4	0	1	1	3	2	2	1	2
$\tilde{\nu}$	1627	1627	1660	1660	1663	1663	1666	1667	1673	1673	1695	1695
ir	3	1	39	49	394	301	650	33	178	696	3	0
R	1	1	10	6	20	1	12	8	5	21	1	2
$\tilde{\nu}$	1695	1695	1705	1706	1708	1708	1730	1730	1733	1734	1742	1742

TABLE 1 (Continued)

ir	0	1	36	27	58	22	21	64	21	112	0	0
R	3	0	17	7	10	13	60	19	56	6	130	131
$\bar{\nu}$	1743	1743	2083	2084	2087	2090	2091	2092	2099	2100	3183	3183
ir	0	0	482	257	213	428	81	191	466	607	30	27
R	166	104	8	40	12	5	35	5	53	40	145	146
$\bar{\nu}$	3188	3188	3195	3195	3202	3202	3260	3260	3266	3266	3270	3270
ir	21	14	10	6	29	3	14	12	7	7	7	6
R	114	179	86	149	38	179	118	183	109	115	108	150
$\bar{\nu}$	3279	3279	3393	3393	3394	3394	3394	3394	3395	3395	3399	3399
ir	5	4	1	1	1	1	2	2	0	0	0	0
R	67	75	46	53	88	49	55	73	66	65	98	79
$\bar{\nu}$	3400	3400	3402	3402	3403	3403	3403	3403	3405	3405	3405	3405
ir	1	1	5	5	5	6	6	6	5	3	5	6
R	123	62	126	120	6	6	63	63	83	36	104	118
$\bar{\nu}$	3405	3405	3410	3410	3415	3415	3415	3415	3431	3432	3592	3592
ir	0	0	0	0	6	5	8	8	3	3	30	29
R	222	212	146	136	304	329	81	404	88	84	60	59
$\bar{\nu}$	3595	3595	3601	3602	3604	3604						
ir	43	78	51	43	27	27						
R	38	69	58	69	33	24						

TABLE 2: Vibrational Wavenumbers and Infrared Intensities of the Model Calculations Described in the Text[a]

no scaling		0.99		0.98	
$\tilde{\nu}$	I	$\tilde{\nu}$	I	$\tilde{\nu}$	I
1638	0.00	1634	0.45	1629	0.75
1638	0.00	1638	0.00	1638	0.00
1646	0.71	1644	0.73	1643	0.72
1646	0.71	1646	0.71	1646	0.71
1654	0.71	1652	0.79	1652	0.89
1654	0.71	1654	0.71	1654	0.71
1662	0.00	1661	0.28	1660	0.40
1662	0.00	1662	0.00	1662	0.00

[a] The C═O stretches of the catenane are obtained by doubling the 4×4 matrix of eq 12 (no scaling) and by subsequently multiplying one diagonal element by 0.99 or by 0.98.

relevant constant of the unperturbed C═O stretch, which is proportional to the square of the wavenumber, and α and β are the mass-weighed interaction force constants. With this simple prescription, the eigenvalues can be calculated even analytically. If one takes $\tilde{\nu} = 1650$ cm^{-1}, $\alpha = D/100$, and $\beta = D/200$, the resulting four wavenumbers are 1638, 1646, 1654, and 1662 cm^{-1}. The associated eigenvectors show that the two central modes are infrared active. The interaction between the four C═O stretches lifts the degeneracy and leads to an increased line width. The introduction of a second noninteracting macrocycle brings about a doubling of each level. A measure of asymmetry is introduced by threading one macrocycle into the cavity of the other. The effect can be mimicked, for instance, by reducing one of the diagonal elements of the eight by eight matrix by 1 or 2% (this agrees with the fact that in the solid only one C═O points inside the ring). We emphasize, however, that this is just a possibility presented here to obtain a qualitative insight into the vibrational dynamics of the system. The effect of asymmetry on the levels of both macrocycles can be readily gathered from the following and will not be treated. Diagonalization yields the results reported in Table 2 where the infrared intensities are calculated assuming that each local oscillator has intensity one and that its contribution to the normal mode intensity is given by the square of its component in the eigenvector. Inspection of the table shows that introduction of the asymmetry redestributes the intensity and spreads even more the active frequencies. Sidebands are predicted to arise at low and high frequencies. In practice, the result is a larger line width for the C═O stretch region. Interestingly, the model also predicts a larger line width for the catenane than for the parent macrocycle.

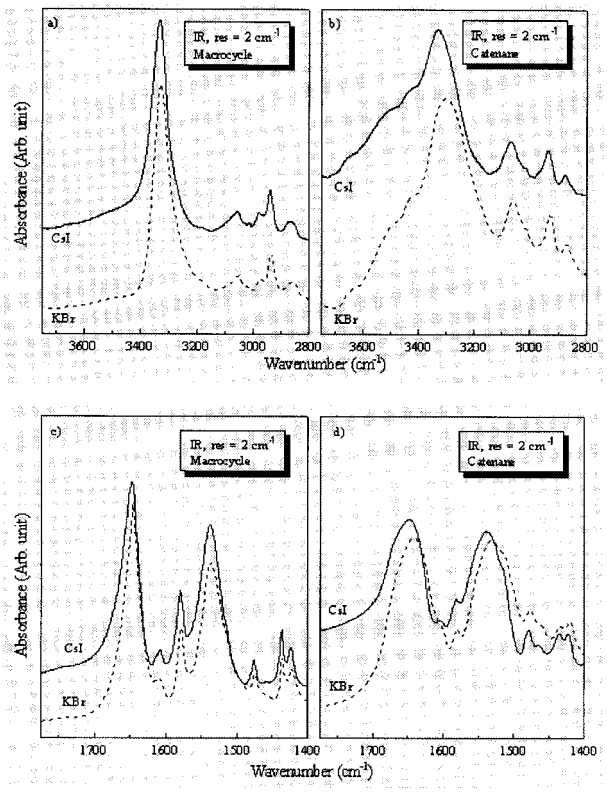

Figure 3. Blowup of selected spectral regions of the infrared spectrum of benzylic amide [2]catenane **1** (b and d) and of its parent macrocyle (a and c) in a KBr and in a CsI matrix.

While the picture presented above is intended to be qualitative, it can be helpul in explaining the experimental observation (see below) that the infrared spectrum of the catenane is quite sensitive to the environment. In the model, the effect of small environmental variations can be simulated by a change of the scaling factor of the diagonal element which, in turn, results in a shift of the center of the spectroscopically active band.

Figure 3 presents two selected regions of the spectra of the catenane and the parent macrocycle in KBr and CsI. We limit the comparison to the amide band II and C═O stretching regions and the N−H stretching region. Remarkably, in the case of the catenane, upon going from KBr to CsI, the amide II and C═O stretching bands are upshifted by 7−8 cm^{-1}, while the NH stretching band is upshifted by 30 cm^{-1}. These frequency shifts are very nearly absent ($\sim$1 cm^{-1}) in the spectra of the parent macrocycle. In agreement with the model, the line width of the spectrum of the catenane is larger than that of the

macrocycle. In the future, we plan to measure the same frequency shifts in a series of salt matrixes for at least two benzylic amide catenanes. These measurements should lead to the development of a quantitative model to understand the phenomenon.

Conclusion

In this work, we have commenced the characterization of the vibrational properties of the simplest member of the family of benzylic amide [2]catenanes. As one might have predicted, in a system of the complexity and the rather low symmetry as the present one, general retrieval of information from the vibrational spectra is not easily accomplished. However, the very nature of the molecule—in which several similar groups interact either via bonds or via space—results in a system with a high sensitivity to the environment. We have found proof of this in the modification of the infrared spectrum of the catenane in KBr and CsI. In the latter environment, the peaks associated to amide band II and the C═O stretchings are downshifted by 8 cm^{-1} while the NH stretching peak is downshifted by 30 cm^{-1}. This behavior is typical of the catenane only and is not present in the macrocycle. A simple qualitative model can rationalize this behavior. We conclude with the final suggestion that the ability to tune this remarkable property of the catenane to modify its vibrational response under rather small perturbations may lead to a vibrationally based sensors.

Acknowledgment. This work has been supported by the European Community, TMR contract FMRX-CT96-0059, and by the Belgian National Program of Interuniversity Research, Project on "Science of Interfaces and Mesoscopic Structures". C.-A.F. acknowledges the FRIA for financial support. P.R. is a senior research assistant of the National Fund for Scientific Research (Belgium).

References and Notes

(1) Schill, G. *Catenanes, Rotaxanes and Knots*. Academic Press; New York, 1971. Sauvage, J.-P. *Acc. Chem. Res.* **1990**, *23*, 319. Amabilino, D. B.; Stoddart, J. F. *Chem. Rev.* **1995**, *95*, 2725. Anelli, P. L.; Spencer, N.; Stoddart, J. F. *J. Am. Chem. Soc.* **1991**, *113*, 5131. Bissell, R. A.; Córdova, E.; Kaifer, A. E.; Stoddart, J. F.; Tolley, M. S. *Nature* **1994**, *369*, 133. Dietrich-Buchecker, C. O.; Livoreil, A.; Sauvage, J.-P. *J. Am. Chem. Soc.* **1994**, *116*, 9399. Collin, J.-P.; Gavinã, P.; Sauvage, J.-P., *Chem. Commun.* **1996**, 2005.

(2) Orlandi, G.; Zerbetto, F.; Zgierski, M. Z. *Chem. Rev.* **1991**, *91*, 867.

(3) Johnston, A. G.; Leigh, D. A.; Pritchard, R. J.; Deegan, M. D. *Angew. Chem., Int. Ed. Engl*. **1995**, *34*, 1209. Johnston, A. G.; Leigh, D. A.; Nezhat, L.; Smart, J. P.; Deegan, M. D. *Angew. Chem., Int. Ed. Engl.* **1995**, *34*, 1212. Johnston, A. G.; Leigh, D. A.; Murphy, A.; Smart, J. P.; Deegan, M. D. *J. Am. Chem. Soc.* **1996**, *118*, 10662. Leigh, D. A.; Moody, K.; Smart, J. P.; Watson, K. J.; Slawin, A. M. Z. *Angew. Chem., Int. Ed. Engl*. **1996**, *35*, 306. Leigh, D. A.; Murphy, A.; Smart, J. P.; Slawin, A. M. Z. *Angew. Chem., Int. Ed. Engl*. **1997,** *36*, 788.

(4) Frisch, M. J.; Trucks, G. W.; Schlegel, H. B.; Gill, P. M. W.; Johnson, B. G.; Wong, M. W.; Foresman, J. B.; Robb, M. A.; Head-Gordon, M.; Replogle, E. S.; Gomperts, R.; Andres, J. L.; Raghavachari, K.; Binkley, J. S.; Gonzalez, C.; Martin, R. L.; Fox, D. J.; Defrees, D. J.; Baker, J.; Stewart, J. J. P.; Pople, J. A. *Gaussian 92/DFT*, Revision G.1; Gaussian, Inc.: Pittsburgh, PA, 1993.

(5) Karna, S. P.; Dupuis, M. *J. Comput. Chem.* **1991**, *12*, 487.

(6) Califano., S. *Vibrational States*; John Wiley & Sons: London, 1976.

(7) Fanti, M.; Orlandi, G.; Zerbetto, F. *J. Phys. B* **1996**, *29*, 5065.

(8) Benz, M.; Fanti, M.; Fowler, P. W.; Fuchs, D.; Kappes, M. M.; Lehner, C.; Michel, R. H.; Orlandi, G.; Zerbetto, F. *J. Phys. Chem.* **1996**, *100*, 13399.

(9) Bellamy, L. J. *Advances in Infrared Group Frequencies*; Methuen and Co. Ltd.: New York, 1968. Alpert, N. L.; Keiser, W. E.; Szymanski, H. A. *Theory and Practice of Infrared Spectroscopy*; Plenum Press: New York, 1970. Socrates, G. *Infrared Characteristic Group Frequencies*; John Wiley and Sons: London, 1980. Lin-Vien, D.; Coltrop, N. B.; Fateley, W. G.; Grasselli, J. G. *The Handbook of Infrared and Raman Characteristic Frequencies of Organic Molecules*, Academic Press: San Diego, CA, 1991.

(10) Dewar, M. J. S.; Thiel, W. *J. Am. Chem. Soc.* **1977**, *99*, 4899.

(11) Christides, C.; Nikolaev, A. V.; Dennis, T. J. S.; Prassides, K.; Negri, F.; Orlandi, G.; Zerbetto F. *J. Phys. Chem.* **1993**, *97*, 3641.

(12) Tarr, A. W.; Zerbetto, F. *Chem. Phys. Lett.*, **1989**, *154*, 273.